Calculations of the Evolution of Ca L_{23} fine structure in Amorphous Calcium Carbonate

Keren Kahil [1], Paolo Raiteri [2], Julian D. Gale [2] and Peter Rez* [3]

1 Department of Structural Biology, Weizmann Institute of Science, Rehovot, 76100, Israel

2 Curtin Institute for Computation/The Institute for Geoscience Research, School of Molecular and Life Sciences, Curtin University, PO Box U1987, Perth, WA 6845, Australia

3 Department of Physics, Arizona State University, Tempe, Arizona, 85287-1504 United States

***** Corresponding Author, Email address: PETER.REZ@asu.edu

Abstract

Amorphous calcium carbonate (ACC) has been found in many different organisms. Biogenic ACC is frequently a precursor in the formation of calcite and aragonite. The process of structural transformation is therefore of great interest in the study of crystallization pathways in biomineralization. Changes in the pre-peak/main peak (L_2'/ L_2) intensity ratio of the Ca L_{23}-edge XAS of Ca-rich particles in skeleton-building cells of sea urchin larva revealed that ACC precipitates through a continuum of states rather than through abrupt phase transitions involving two distinct phases as hitherto believed. Using an atomic multiplet code, we show that only a tetragonal or "umbrella-like" distortion of the Ca coordination polyhedron can give rise to the observed continuum of states. We also show, based on structures obtained from previous molecular dynamics simulations of hydrated nanoparticles, that the Ca L_{23}-edge is not sensitive to atomic arrangements in the early stages of the transformation process.

Introduction

Amorphous calcium carbonate (ACC) is very significant in the growth of biogenic $CaCO_3$ minerals as it often serves as the precursor to the formation of the crystalline phases [1,2]. Since it was identified as a precursor for calcite in the sea urchin spicule [3], ACC precursor phases to calcite or aragonite have been observed in various organisms from different phyla [4-12]. The transformation of ACC to either calcite or aragonite has increased interest in how the short-range order, as defined by the coordination of oxygen around the calcium ions, controls the mineralization process.

X-ray absorption spectroscopy (XAS), either by Extended X-ray Absorption Fine Structure (EXAFS) of the Ca K absorption edge or by X-ray Absorption Near Edge Structure (XANES) of both the Ca K-edge and the Ca $L_{2,3}$-edge, is frequently used to study the coordination of cations in minerals [13-15]. The Ca $L_{2,3}$-XANES spectra of $CaCO_3$ minerals, according to simulations and theory, is sensitive to changes both in the symmetry of the Ca-O coordination polyhedron and in the relative orientation of the polyhedra [16-18].

Using both XANES and EXAFS, several ACC phases were discovered [13, 14, 19]. Among these phases, two transient ACC phases were detected in the sea urchin larval spicule [14]. The first is short-lived and similar to hydrated synthetic ACC, where nanoparticles of calcium carbonate surrounded by water represents a plausible model for this phase[20, 21]. This ACC rapidly transforms by dehydration into a second amorphous phase, which is believed to be similar to anhydrous synthetic ACC. The latter transforms more slowly into biogenic calcite. Thus the prevailing paradigm, until recently, in both the sea urchin larval spicule and, to some extent, also in the general field of biogenic ACC, was of two ACC phases and a three stage biomineralization process where hydrated ACC transformed to anhydrous ACC and then to calcite.

In a recent study, we used cryo-soft X-ray microscopy (SXM) to detect Ca-rich moieties in skeleton-building cells of sea urchin larvae. Using cryo-SXM we observed hundreds of intracellular Ca-rich particles and measured their Ca L_{23}-edge XANES [22]. We calculated

the ratio of heights of the L_2 pre-peak (L_2') to the main L_2 peak (L_2'/L_2) (see Fig 1A for peak definition) of each particle as this ratio correlates with the stage of ACC transformation. We used the L_2 features in our analysis since the signal/noise for the ratio of the L_2 pre-peak to the main peak was higher than the signal/noise for the comparable feature on the L_3 peak. The L_2'/L_2 values of the three previously identified calcium carbonate phases in the sea urchin larval spicule are 0.26 for hydrated ACC, 0.4 for anhydrous ACC and 0.45 for calcite. The results we obtained in our recent study of the intracellular Ca-rich particles showed a continuum of disordered states, with L_2'/L_2 values of particles ranging from 0.13, much lower than hydrated ACC, to 0.4, which is similar to anhydrous ACC. In an investigation of the dehydration of synthetic ACC, Tsao *et al.* measured the splitting between the L_2' pre-peak and the L_2 main peak with temperature under conditions of 1.3% relative humidity[21]. They did not observe any change in the splitting as the ACC transformed from a hydrated to an anhydrous phase.

The fine structure in the L_3 and L_2 absorption peaks is related to the arrangements of the oxygen anions around the Ca cation. In earlier work, atomic multiplet theory was shown to give excellent agreement with the fine structure observed in both calcite and aragonite, and could also explain the structural distortions that might be responsible for the fine structure observed both in anhydrous and hydrated ACC [16]. A plausible model of the transformation process was then proposed based on these distortions. A limitation of the earlier work is that the code used, CTM4XAS [23,24], only permitted crystal field interactions based on group theory and would only allow for distortions consistent with either C_{4v} or D_{4h} symmetry around the Ca ion. To explore a wider range of possibilities in this work we have used the code of Uldry *et al*. [25], which accounts for the crystal field by explicitly calculating the electrostatic interactions from the neighboring ions modeled as point charges and has no symmetry restrictions. We were particularly interested in distortions that can give rise to a continuous range of L_2'/L_2 values. These are relevant for the later stages of the transformation process where the anhydrous phase transforms to calcite. We examined several options and observed that the tetragonal distortion where the atoms at the apices of the polyhedron move inwards and the other

atoms move outwards gives a linear variation in the L_2'/L_2 ratio, as does a distortion where the atoms in the x,y plane move upwards with respect to the apical atoms. We call this latter distortion an "umbrella" distortion and in some ways it is similar to the distortion shown as Fig. 3 in Rez and Blackwell [16] (Supplementary Information, Fig. S1).

To investigate whether the L_2 pre-peak to main peak ratio gives useful information on the early stages of the transformation involving formation of hydrated ACC we calculated spectra for nano-crystalline models previously developed by Raiteri and Gale [26]. They considered a range of nanoparticle sizes from 90 to 864 $CaCO_3$ units with varying degrees of initial hydration. It should be noted that in the approach taken in their earlier work, water was introduced into the ACC structure in a manner that led to a relatively homogeneous distribution[15], the atomic structure is shown in Supplementary Information, Fig. 2A and B. In contrast, in their more recent work [27], small dry ACC nanoparticles (36 formula units) were arranged in a 3D lattice and intercalated with water to mimic the presence of channels of water, as was proposed by Goodwin *et al.*[28] (hereafter referred to as "heterogeneous" based on the water distribution, to differentiate it from the more homogeneous nanoparticles of the earlier work) shown in Supplementary Information, Fig. 2C. As a comparison, the same 36 formula unit ACC nanoparticles were used to build a 3D ACC dry structure [27]. Note that water molecules can cover the surface of these dry nanoparticles. The models have some similarity to the nanoparticle models of Rez *et al.*[20] used to explain the diffraction profiles from both synthetic and biogenic ACC. During these earlier studies molecular dynamics (MD) was used to locally equilibrate the system, recognizing that exploration of the full configuration space would occur on a timescale well beyond that accessible to unbiased simulation. In this work, we took the final structures of these nanoparticles and ran short MD simulations with a more recent $CaCO_3$ force field [29]. This should give a more realistic representation of any distortion of the carbonate anion because it does not use a rigid description of this species, unlike the earlier model used in Raiteri and Gale, and the vibrational frequencies of carbonate were used during the parameterization of the flexible force field. The simulations were run at 300 K for a few hundred ps with a time

step of 1 fs using LAMMPS [30]. Again, we note that the objective was to only relax the structure in response to the change of forcefield, rather than to re-explore configuration space. The arrangements of oxygen ions within 2.8 Å of each Ca ion were extracted as separate files to be used for the calculation of the XANES spectra, which were averaged over all the extracted configurations. Note that the ACC structures from Huang *et al*.[27] included one bicarbonate ion, which in this work has been converted to a carbonate to maintain charge neutrality in the system.

In the above nanoparticle models, the coordination of oxygen ions around the calcium ions was described by the distribution of bond lengths, bond angles and even coordination number, and not just by a particular symmetry. Using the code of Uldry *et al*.[25] we simulated the Ca $L_{2,3}$-edge spectra that would be observed from the range of nanoparticle structures generated here. The fine structures were consistent with the highly disordered and fully hydrated form of ACC with some indication of the L_2' peak emerging from models based on small heterogeneous nanoparticles. However, given the low value of the pre-peak to main peak intensity, the Ca L_2 fine structure is not sensitive to details of nanoparticle structure. This confirms the view that the structures obtained from MD simulations only represent the initial stage of the dehydration process.

Results

Our starting point for the calculation of spectra was to find the parameters that give the best goodness of fit (χ^2 test, explained in SI, supplementary methods) between the experimental and calculated XANES spectra of calcite and aragonite, as well-defined reference systems; these are summarized in Table 1. The corresponding spectra for calcite and aragonite with these parameters are shown in Figure 1 A, C. The separation between the L_2 and L_3 peaks is controlled by the spin-orbit splitting and the Coulomb interaction parameters, the split between the pre-peaks and the main peaks is controlled by the effective charge of the coordinating atoms and the crystal field. As discussed in Uldry *et al*. [25], the matrix elements of the Coulomb interaction, the spin-

orbit coupling and the crystal field were scaled to match the experimental measurement. The broadening was chosen to match the resolution achievable in synchrotron-based XAS. Scaling the effective charge in a model with fixed charges at point atoms is only an approximation to the charge distribution in a solid that should be calculated by density functional theory. In aragonite there are 9 oxygen atoms in a 1st coordination shell with a range of distances from 2.42 to 2.69 Å, followed by a 2nd coordination shell of C atoms with a range of distances from 2.9 to 3.4 Å. Good agreement for aragonite could be obtained with an oxygen charge of -2.0. Adding the 2nd coordination shell with Carbon atoms with a charge of +1.0 made very little difference. The aragonite parameters were therefore considered appropriate for the disordered nanoparticle structures representing the early stages of transformation of ACC described by the nanoparticle models. In calcite the Ca are coordinated by 6 oxygen atoms in the 1st shell at 2.35 Å, followed by 6 Carbon in a 2nd shell at 3.21 Å and 6 more oxygen in a 3rd shell at 3.46 Å. With the same charges as used for aragonite, it was necessary to include all 3 coordination shells for the relative peak heights to better match the experimental measurement in this more ordered structure (Fig 1B). Choosing an effective charge of -1.2 for the oxygen in the 1st coordination shell has the same effect as summing over the different coordination shells with alternating charges (Figure 1A). The calcite parameters listed in Table 1 were used for calculations for distortions from the calcite structure representing the later stages of transformation of ACC to calcite. We note that the experimental intensity is greater than the theoretical estimate at energies above the L_2 peak, 353-356 eV, as the transitions to continuum states have not been included in our calculation.

Table 1 – Best fit parameters for calculation of XANES spectra using the code of Uldry *et al*. code [25]

Parameter	Calcite	Aragonite
Coulomb interaction scaling *	0.75	0.7
Crystal field scaling *	1.16	0.8
Spin-orbit scaling *	0.91	0.9
Core-hole lifetime Lorentzian broadening *	0.15	0.15
Effective charge of Oxygen atoms	-1.2	-2
χ^2	0.003	0.002

* Parameters are in eV

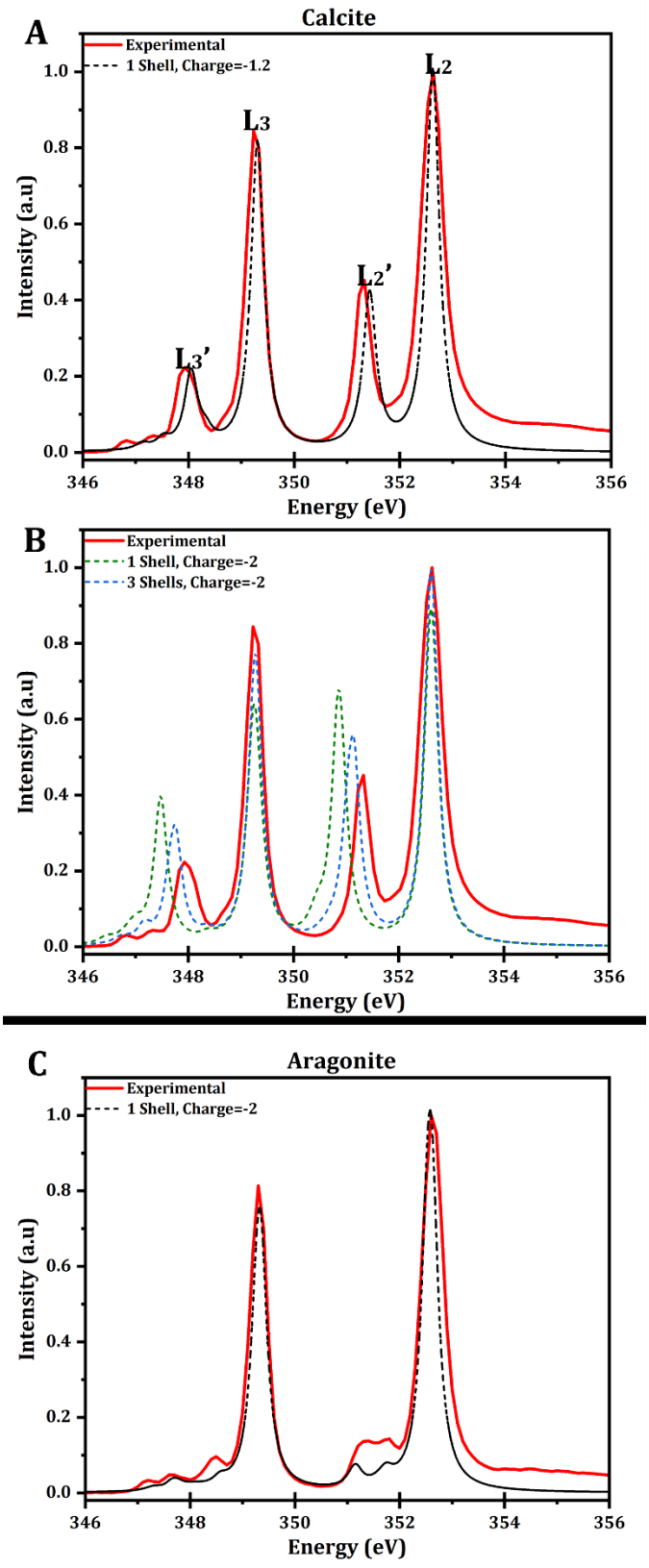

Figure 1. Comparison between simulated (dashed line) and experimental (solid line) spectrum of Ca-$L_{2,3}$ XANES. (A) Simulation of calcite with 1st coordination shell and oxygen effective charge of -1.2. (B) Simulation of calcite with oxygen effective charge of -2 and 1st (green) and 3rd (blue) coordination shell. (C) Simulation of aragonite with 1st coordination shell and oxygen effective charge of -2.

After achieving good agreement for both calcite and aragonite, we turned to the results for the ACC nanoparticles previously created by Raiteri and Gale with varying sizes and degrees of hydration [26, 27]. Using the atomic coordinates from their simulated nanoparticles, after annealing with the updated force field model, we calculated, using the aragonite parameters, the Ca-$L_{2,3}$ XANES averaged for all the calcium ions in the final nanoparticle configuration of the MD simulations. No difference was observed when the configurations of the final 9 frames of the trajectory sampled every 250 ps were used.

We considered $CaCO_3$ nanoparticles with 864 formula units and a homogeneous water distribution. Two initial hydration states were investigated; one was a hydrated state (wet) with a ratio of water to $CaCO_3$ of 1.3 and the other a partially dehydrated (dry) nanoparticle with a ratio of water to $CaCO_3$ of 0.4. As all of the nanoparticles examined gave spectra that resemble aragonite more than ACC or calcite, as shown in Fig. 2a, we conclude that the structures from the work of Raiteri and Gale [26], which have a relatively uniform distribution of water, represent the very early stages of ACC evolution. This should not be surprising. An analysis of oxygen coordination shows a substantial number of cases of 7-fold and 8-fold coordination for calcium, as shown in Fig. 3 Ai and Bi. This is somewhat less than the 9-fold coordination of calcium by oxygen in aragonite, but much greater than the 6-fold coordination found in calcite. We note for comparison that in water Ca^{2+} typically exhibits between 6- and 8-fold coordination, with the average being close to 7-fold[29, 31, 32]. The distribution of bond lengths (Fig. 3Aii and Bii) is also quite broad, about 0.3 Å wide. The distribution of the bond lengths is slightly asymmetric as packing constraints limit the possibility of shorter bond lengths. The distribution of bond angles has peaks at 51°, 77° and 123° (Fig. 3Aiii and Bii), which is hard to reconcile with any structure based on small distortions from the near perfect octahedral symmetry of calcite.

We then calculated spectra based on the 36 formula unit nanoparticles as generated by Huang *et al.* [27]. A feature corresponding to the L_2' pre peak can be seen to begin to emerge in the heterogeneous nanoparticles. This is also apparent in spectra acquired by Tsao et al [31] at a relative humidity of 1.3%. Although the bond length distributions (Figs.

3Cii, 3Dii) are similar to the bond length distributions from the homogeneous nanoparticles, the peaks in the bond angle distribution at 51° and 123° are suppressed (Figs. 3Ciii, 3Diii) and there is a much wider range of coordination (Fig 3Ci,3Di).

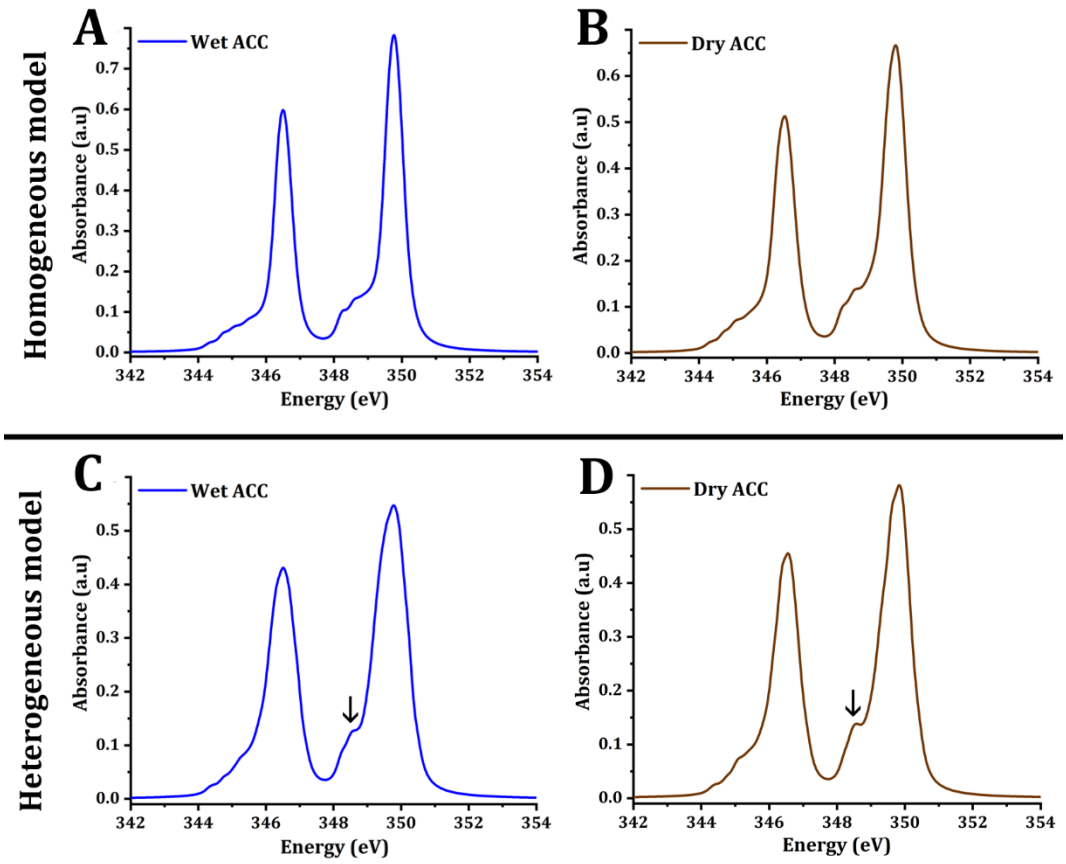

Figure 2. Averaged Ca-$L_{2,3}$ XANES simulation of 4 $CaCO_3$ nanoparticles compared to experimental spectra. (A,B) nanoparticles from the homogenous model with 864 formula units [26]. (A) Nanoparticle with initial H_2O to $CaCO_3$ ratio of 1.3. (B) Nanoparticle with initial H_2O to $CaCO_3$ ratio of 0.4. (C) hydrated (wet) and (D) dehydrated (dry) nanoparticles from the heterogeneous model [27]. Arrows pointing to the emerging L_2' feature.

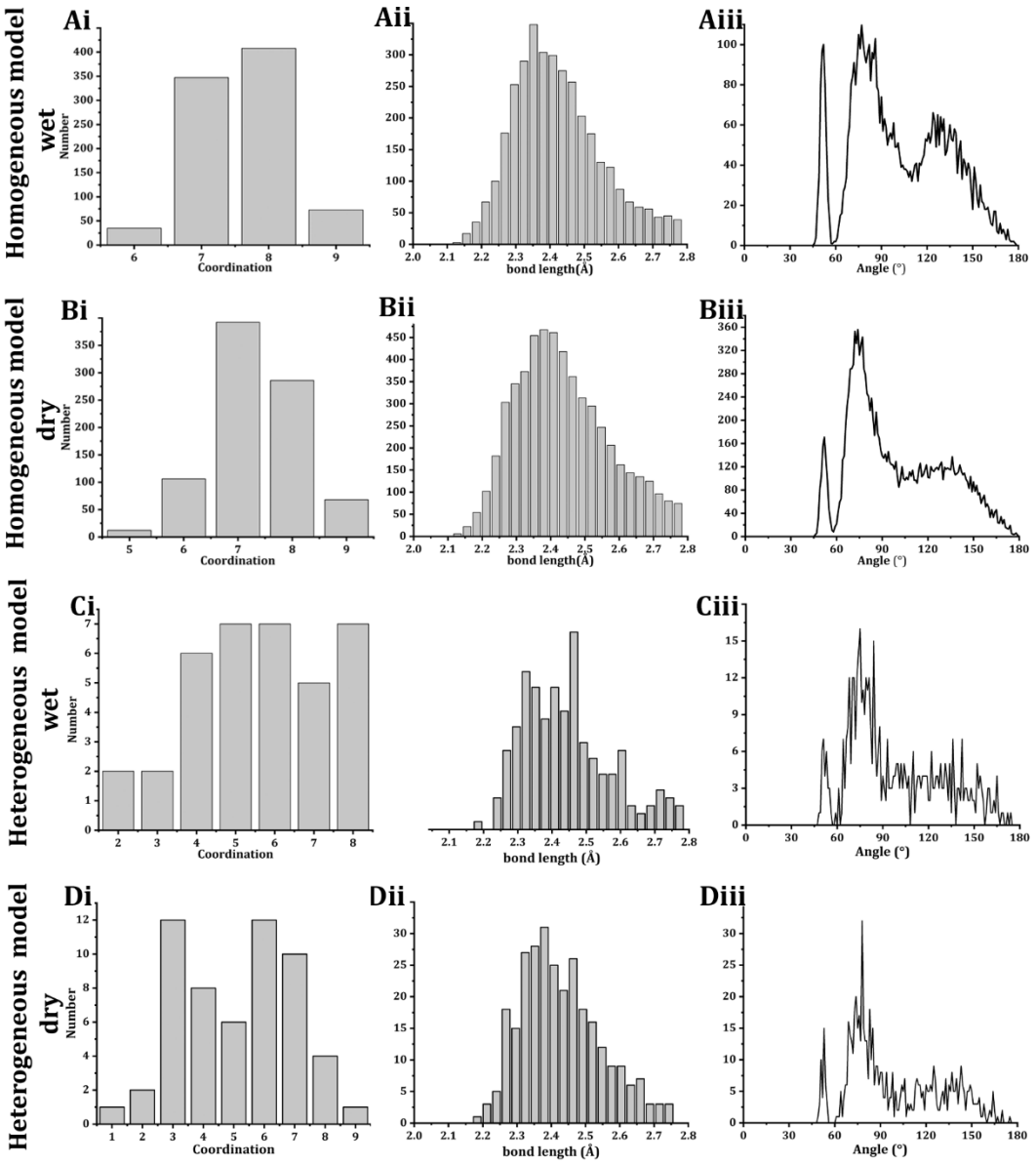

Figure 3. Distribution of (i) coordination number of oxygen around calcium (ii) Ca-O bond lengths and (iii) distribution of angles between Ca-O bonds. The distributions are presented for (A) nanoparticle with 864 formula unit nanoparticle and an initial H_2O to $CaCO_3$ ratio of 1.3 (wet) from the homogenous model. (B) nanoparticle with 864 formula unit nanoparticle and an initial H_2O to $CaCO_3$ ratio of 0.4 (dry) from the homogenous model. (C)hydrated (wet) nanoparticle from the heterogeneous model and (D) dehydrated (dry) nanoparticle from the heterogeneous model.

The next step was exploring several possible distortions of the oxygen polyhedron. We changed Ca-O bond lengths of each oxygen atom randomly between calcite and aragonite bond lengths, while randomly changing the angles of the Ca-O bonds relative

to the x and y axes, $(Ca\text{-}O)_{xy}$ bonds. These random changes were done without fixing the structure by symmetry and reducing the symmetry according to D_{4h} and C_{4v}, as depicted in Rez and Blackwell's paper in Fig. 3 [16], reproduced as Supplementary Figure S1. Although it was possible to match spectra from hydrated ACC and aragonite, it was not possible to generate a linear trend in the L_2'/L_2 ratio with respect to the magnitude of the distortion (Table S1 and Table S2).

We continued to explore the Ca-O coordination polyhedron distortions suggested by Rez and Blackwell [16], reducing the symmetry of the calcite octahedron to a tetragonal symmetry as shown in Fig. 4A. We systematically changed the ratio between the $(Ca\text{-}O)_{xy}$ bond length and the Ca-O bond lengths projected along the z axis, $(Ca\text{-}O)_z$, comparable to the process performed by Gueta *et al.* [33]. This change resulted in a gradual and continuous change in the L_2'/L_2 values (Fig. 4B). The minimum value of the L_2'/L_2 ratio was for a small elongation in the z direction when $(Ca\text{-}O)_z/(Ca\text{-}O)_{xy}$=1.01. We then kept this ratio constant and changed $(Ca\text{-}O)_{xy}$ bond length (Fig. 4C). This distortion proved valuable as it resulted in a wide range of L_2'/L_2 starting from 0.2 (lower than hydrated ACC). Examplary spectra can are found in the Supplamentry Information, figure S3.

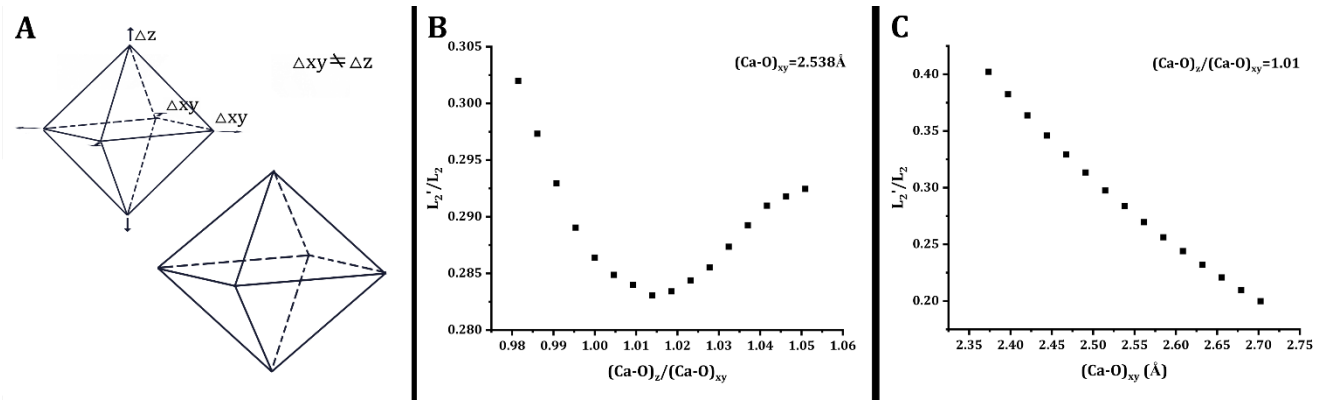

Figure 4. Tetragonal distortion to the coordination polyhedron and its impact on L_2'/L_2. (A) A schematic drawing of the changes in the oxygen positions, the upper left drawing is a octahedron and the lower right drawing is the distorted polyhedron, which now has a tetragonal symmetry. (B) L_2'/L_2 values obtain from Ca-$L_{2,3}$ XANES generated for $(Ca\text{-}O)_{xy}$=2.537Å (1.08 times that of calcite) and various $(Ca\text{-}O)_z/(Ca\text{-}O)_{xy}$ ratios. (C) L_2'/L_2 values obtain from Ca-$L_{2,3}$ XANES generated for $(Ca\text{-}O)_z/(Ca\text{-}O)_{xy}$=1.01 and various $(Ca\text{-}O)_{xy}$.

A similar trend was also obtained by creating an umbrella-like distortion, changing uniformly the angle between the atoms originally in the xy plane and the z axis (Fig. 5). In this case, we kept the bond distances the same as in calcite.

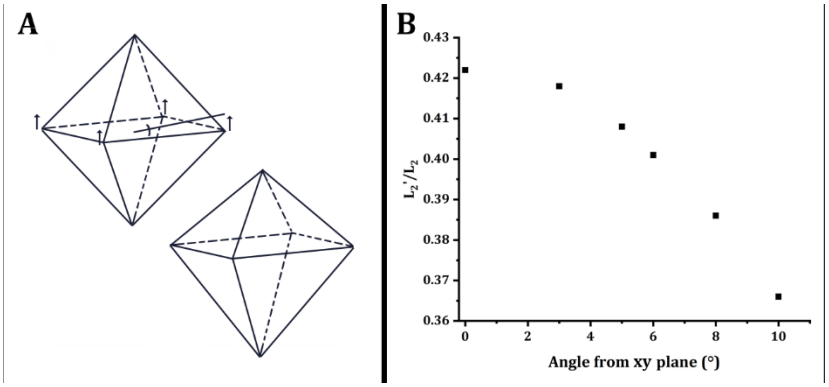

Figure 5. "Umbrella" distortion. (A) A schematic drawing of the changes in the oxygen positions, the upper left drawing is a octahedron and the lower right drawing is the distorted polyhedron. (B) L_2'/L_2 values obtain from Ca-$L_{2,3}$ XANES generated for displacing the oxygens originally located in the xy plane, by a few degrees relative to the xy plane, while keeping $(Ca\text{-}O)_{xy}$ constant.

Discussion and conclusions

In this study, we tested several possible atomic configurations of the oxygen coordination polyhedron around the Ca atom in calcium carbonate minerals. Our aim was to explain the continuum of short-range disordered states of ACC observed in the sea urchin larval spicule-forming cells measured by soft X-ray microscopy [12]. Two main distortions to the oxygen polyhedron resulted in a continuous range of L_2'/L_2 values, a reduction in symmetry from octahedral to tetragonal and the "umbrella" distortion. Our results reinforce the conclusion made by Kahil *et al*. that the process of ACC precipitation occurs with no abrupt phase transitions of whole $CaCO_3$ nano-particles [22]. The combination of both studies provides a clarification, from the atomic point of view, as to the nature of the deposition process of ACC, including the transition between the hydrated and anhydrous ACC phases, which takes place in a gradual manner with several possible distortions to the oxygen polyhedron.

Multiplet calculations with the code of Uldry *et al*. allow for a wider range of oxygen coordination possibilities around the Ca ion, not limited to particular symmetries [25]. This meant that it was possible to explore theoretical models, such as those arising from the MD simulations, describing both the earlier stages of the transformation process where water distribution is likely to be more homogeneous as well as the later stages where it is more probable that distinct nanoparticles have formed with residual water located in voids between them. Our calculations showed that the XANES spectra and the L_2'/L_2 ratio for the early stages were consistent with a disordered local environment similar to aragonite. The calculated spectra from the model based on discrete nanoparticles with a heterogeneous water distribution shows signs of the emergence of the L_2' pre peak, also observed by Tsao et al [31] in spectra acquired at a relative humidity of 1.3%. It is interesting to note that this model is consistent with the structures proposed by Rez et al. to explain diffraction profiles from synthetic and biogenic ACC [20]. However, the L_2'/L_2 ratio is a very sensitive measure of distortion of the coordination polyhedron in the later stages of the transformation process, and there appears to be a linear relationship between the L_2'/L_2 ratio and the degree of distortion. By itself, this measure cannot be

used to distinguish between the “tetragonal” distortion and the “umbrella” distortion. However, these new results are still consistent with the transformation mechanism to calcite proposed by Rez and Blackwell [16]. In the initial stages the coordination polyhedral are highly distorted with random orientations. They then go through a phase with the “tetragonal” or “umbrella” distortion, but randomly oriented around the apical (z) axis. The final stage is the disappearance of the distortion and the alignment and ordering of the polyhedra.

Acknowledgements

Authors Raiteri and Gale thank the Pawsey Supercomputing Centre and National Computational Infrastructure for the provision of computing resources. JDG acknowledges the ARC for funding under grant FL180100087. Prof. Rez would like to thank Dr. Sirong Lu for making him aware of the code of Uldry *et al*. (ref. 10), and Mr. Adam Siegel for help with the calculations. The authors would like to thank Prof. Lia Addadi and Prof. Steve Weiner for inspiration and fruitful discussions.

Supporting Information

Supplementary tables S1 and S2, supplementary figures S1, S2 and S3, together with supplementary methods are found in Supporting Information.

References

(1) Addadi, L.; Vidavsky, N.; Weiner, S. Transient precursor amorphous phases in biomineralization. In the footsteps of Heinz A. Lowenstam. *Z. Kristallogr. Cryst. Mater.* **2012**, *227* (11)

(2) 711-717. Addadi, L.; Raz, S.; Weiner, S. Taking advantage of disorder: Amorphous calcium carbonate and its roles in biomineralization. *Adv. Mater.* **2003**, *15* (12), 959-970. DOI: 10.1002/adma.200300381.

(3) Beniash, E.; Aizenberg, J.; Addadi, L.; Weiner, S. Amorphous calcium carbonate transforms into calcite during sea urchin larval spicule growth. *Proc. R. Soc. Lond., B, Biol. Sci.* **1997**, *264* (1380), 461-465.

(4) Weiss, I. M.; Tuross, N.; Addadi, L.; Weiner, S. Mollusc larval shell formation: Amorphous calcium carbonate is a precursor phase for aragonite. *J. Exp. Zool.* **2002**, *293* (5), 478-491. DOI: 10.1002/jez.90004.

(5) Akiva, A.; Neder, M.; Kahil, K.; Gavriel, R.; Pinkas, I.; Goobes, G.; Mass, T. Minerals in the pre-settled coral Stylophora pistillata crystallize via protein and ion changes. *Nat. Commun.* **2018**, *9* (1), 1-9.

(6) Rodríguez-Navarro, A. B.; Marie, P.; Nys, Y.; Hincke, M. T.; Gautron, J. Amorphous calcium carbonate controls avian eggshell mineralization: a new paradigm for understanding rapid eggshell calcification. *J. Struct. Biol.* **2015**, *190* (3), 291-303.

(7) Macías-Sánchez, E.; Willinger, M. G.; Pina, C. M.; Checa, A. G. Transformation of ACC into aragonite and the origin of the nanogranular structure of nacre. *Sci. Rep.* **2017**, *7* (1), 1-11.

(8) Hasse, B.; Ehrenberg, H.; Marxen, J. C.; Becker, W.; Epple, M. Calcium carbonate modifications in the mineralized shell of the freshwater snail Biomphalaria glabrata. *Eur. J. Chem.* **2000**, *6* (20), 3679-3685.

(9) Politi, Y.; Arad, T.; Klein, E.; Weiner, S.; Addadi, L. Sea urchin spine calcite forms via a transient amorphous calcium carbonate phase. *Science* **2004**, *306* (5699), 1161-1164.

(10) Dillaman, R.; Hequembourg, S.; Gay, M. Early pattern of calcification in the dorsal carapace of the blue crab, Callinectes sapidus. *J. Morphol.* **2005**, *263* (3), 356-374.

(11) Lee, M.; Hodson, M.; Langworthy, G. Crystallization of calcite from amorphous calcium carbonate: Earthworms show the way. *Mineral. Mag.* **2008**, *72* (1), 257-261.

(12) DeVol, R. T.; Sun, C.-Y.; Marcus, M. A.; Coppersmith, S. N.; Myneni, S. C.; Gilbert, P. U. Nanoscale transforming mineral phases in fresh nacre. *J. Am. Chem. Soc* **2015**, *137* (41), 13325-13333.

(13) Levi-Kalisman, Y.; Raz, S.; Weiner, S.; Addadi, L.; Sagi, I. Structural differences between biogenic amorphous calcium carbonate phases using X-ray absorption spectroscopy. *Adv. Funct. Mater.* **2002**, *12* (1), 43-48.

(14) Politi, Y.; Metzler, R. A.; Abrecht, M.; Gilbert, B.; Wilt, F. H.; Sagi, I.; Addadi, L.; Weiner, S.; Gilbert, P. U. P. A. Transformation mechanism of amorphous calcium carbonate into calcite in the sea urchin larval spicule. *Proc. Natl. Acad. Sci.* **2008**, *105* (45), 17362-17366. DOI: 10.1073/pnas.0806604105.

(15) Cartwright, J. H.; Checa, A. G.; Gale, J. D.; Gebauer, D.; Sainz-Díaz, C. I. Calcium carbonate polyamorphism and its role in biomineralization: How many amorphous calcium carbonates are there? *Angew. Chem. Int. Ed.* **2012**, *51* (48), 11960-11970.

(16) Rez, P.; Blackwell, A. Ca L_{23} spectrum in amorphous and crystalline phases of calcium carbonate. *J. Phys. Chem. B* **2011**, *115* (38), 11193-11198. DOI: 10.1021/jp203057y.

(17) De Groot, F.; Fuggle, J.; Thole, B.; Sawatzky, G. $L_{2,3}$ x-ray-absorption edges of d 0 compounds: K^{+}, Ca^{2+}, Sc^{3+}, and Ti^{4+} in O_h (octahedral) symmetry. *Phys. Rev. B* **1990**, *41* (2), 928.
(18) Himpsel, F.; Karlsson, U. O.; McLean, A.; Terminello, L.; De Groot, F.; Abbate, M.; Fuggle, J.; Yarmoff, J.; Thole, B.; Sawatzky, G. Fine structure of the Ca 2p X-ray-absorption edge for bulk compounds, surfaces, and interfaces. *Phys. Rev. B* **1991**, *43* (9), 6899.
(19) Mass, T.; Giuffre, A. J.; Sun, C.-Y.; Stifler, C. A.; Frazier, M. J.; Neder, M.; Tamura, N.; Stan, C. V.; Marcus, M. A.; Gilbert, P. U. P. A. Amorphous calcium carbonate particles form coral skeletons. *Proc. Natl. Acad. Sci.* **2017**, *114* (37), E7670-E7678. DOI: 10.1073/pnas.1707890114.
(20) Rez, P.; Sinha, S.; Gal, A. Nanocrystallite model for amorphous calcium carbonate. *J. Appl. Crystallogr.* **2014**, *47* (5), 1651-1657.
(21) Tsao, C.; Yu, P.-T.; Lo, C.-H.; Chang, C.-K.; Wang, C.-H.; Yang, Y.-W.; Chan, J. C. C. Anhydrous amorphous calcium carbonate (ACC) is structurally different from the transient phase of biogenic ACC. *Chem. Commun.* **2019**, *55* (48), 6946-6949.
(22) Kahil, K.; Varsano, N.; Sorrentino, A.; Pereiro, E.; Rez, P.; Weiner, S.; Addadi, L. Cellular pathways of calcium transport and concentration toward mineral formation in sea urchin larvae. *Proc. Natl. Acad. Sci.* **2020**, *117* (49), 30957-30965. DOI: 10.1073/pnas.1918195117.
(23) De Groot, F. Multiplet effects in X-ray spectroscopy. *Coord. Chem. Rev.* **2005**, *249* (1-2), 31-63.
(24) Thole, B.; Van der Laan, G.; Fuggle, J.; Sawatzky, G.; Karnatak, R.; Esteva, J.-M. 3d x-ray-absorption lines and the $3d^9\ 4f^{n+1}$ multiplets of the lanthanides. *Phys. Rev. B* **1985**, *32* (8), 5107.
(25) Uldry, A.; Vernay, F.; Delley, B. Systematic computation of crystal-field multiplets for X-ray core spectroscopies. *Phys. Rev. B* **2012**, *85* (12), 125133.
(26) Raiteri, P.; Gale, J. D. Water is the key to nonclassical nucleation of amorphous calcium carbonate. *J. Am. Chem. Soc* **2010**, *132* (49), 17623-17634.
(27) Huang, Y.-C.; Rao, A.; Huang, S.-J.; Chang, C.-Y.; Drechsler, M.; Knaus, J.; Chan, J. C.; Raiteri, P.; Gale, J. D.; Gebauer, D. Uncovering the role of bicarbonate in calcium carbonate formation at near-neutral pH. *Angew. Chem. Int. Ed.* **2021**.
(28) Goodwin, A. L.; Michel, F. M.; Phillips, B. L.; Keen, D. A.; Dove, M. T.; Reeder, R. J. Nanoporous structure and medium-range order in synthetic amorphous calcium carbonate. *Chem. Mater.* **2010**, *22* (10), 3197-3205.
(29) Raiteri, P.; Demichelis, R.; Gale, J. D. Thermodynamically consistent force field for molecular dynamics simulations of alkaline-earth carbonates and their aqueous speciation. *J. Phys. Chem C* **2015**, *119* (43), 24447-24458.
(30) Plimpton, S. Fast parallel algorithms for short-range molecular dynamics. *J. Comput. Phys.* **1995**, *117* (1), 1-19.
(31) Ohtaki, H.; Radnai, T. Structure and dynamics of hydrated ions. *Chem. Rev.* **1993**, *93* (3), 1157-1204.
(32) Raiteri, P.; Schuitemaker, A.; Gale, J. D. Ion pairing and multiple ion binding in calcium carbonate solutions based on a polarizable AMOEBA force field and ab initio molecular dynamics. *J. Phys. Chem B* **2020**, *124* (17), 3568-3582.
(33) Gueta, R.; Natan, A.; Addadi, L.; Weiner, S.; Refson, K.; Kronik, L. Local atomic order and infrared spectra of biogenic calcite. *Angew. Chem. Int. Ed.* **2007**, *46* (1-2), 291-294.

TOC graphics